Journal of Materials Science: Materials in Electronics (2020) 31:7905–7915
https://doi.org/10.1007/s10854-020-03329-3

Use of redox additive to enhance the electrochemical performance of Co_3O_4/polyaniline/graphene composite-based supercapacitors

Prasenjit Haldar[1]

Received: 12 January 2020 / Accepted: 26 March 2020 / Published online: 4 April 2020

Abstract
The synthesized ternary composite Co_3O_4/polyaniline/graphene delivered high capacitance of ~ 476 F g^{-1} at a current density of 2 A g^{-1}, within the voltage window from − 0.8 to 0.8 V in three-electrode configuration. The symmetric device, fabricated using the composite material returned specific capacitance of ~ 37 F g^{-1} at a current density of 0.5 A g^{-1}. Further, the effect of redox additive KI in electrolyte 1 M Na_2SO_4 was investigated in symmetric device configuration. The optimum results were obtained when 75 mmol KI was added with 1 M Na_2SO_4 electrolyte and capacitance increased more than two times, compared to the case while no redox additive was added in electrolyte and the maximum capacitance was found to be ~ 94 F g^{-1}, at a current density 1 A g^{-1}.

1 Introduction

The necessity of energy storage devices in daily lives is ever increasing. Among the energy storage devices, supercapacitors and their variations (e.g. superbats, Na-ion supercapacitors, Li-ion supercapacitors etc.) are well accepted in various applications. There are recent reports which showed the variation of the performance of electrochemical energy storage devices under non-ideal conditions [1–4]. But, the focus on finding low-cost electrode materials with high capacitance and cycling stability must go on. It is also important to concentrate on different varieties of materials, using every possible or feasible information that are available till now and find effective strategies to develop electrode materials that may have superior characteristics compared to the conventional electric double layer capacitor (EDLC) and pseudocapacitor types of materials. Operating voltage window plays a significant role in ensuring practical application of supercapacitors. Though, non-aqueous organic, ionic liquids and gel-polymer electrolytes provide high operating voltage window, they return low capacitance values compared to aqueous electrolytes. There is also need for revisiting proper voltage windows for electrode materials, especially in aqueous neutral electrolytes, as there are few reports which suggests that it is possible to extend the operating voltage window using the neutral electrolytes [5, 6]. It is also essential to find easy synthesis routes which will produce low CO_2 footprints hence reduce the negative impact on the environment [7].

Different types of binary and ternary composites are previously reported as a way to enhance the capacitance value and cycling stability of supercapacitor by taking account the individual property of materials. The binary composites are generally composed in the combination of (a) pseudocapacitive material and EDLC material or (b) two pseudocapacitive materials. The ternary composites are prepared in the combination of (a) two pseudocapacitive materials and one EDLC material or (b) two EDLC materials and one pseudocapacitive material or (c) addition of metal with pseudocapacitive and EDLC type materials [8–22].

In this present work, the individual property of metal oxide, polyaniline (PANI) and graphene were used to synthesize material which would cumulatively show high capacitance value and high cycling stability. Metal oxide Co_3O_4 was used due to its high theoretical capacitance value (3560 F g^{-1}), low cost and environmental friendliness [23–25]. It is possible to prepare Co_3O_4 with different morphologies including nanoparticles, nanorods, nanowires, quasi-cubes, nanosheets and porous nanostructures etc. [24–31]. The

Electronic supplementary material The online version of this article (https://doi.org/10.1007/s10854-020-03329-3) contains supplementary material, which is available to authorized users.

✉ Prasenjit Haldar
prasenjit94744@gmail.com

[1] Department of Physics, Indian Institute of Technology Kharagpur, Kharagpur, West Bengal 721302, India

performance of supercapacitors using Co_3O_4 depend on its morphology. Though, Co_3O_4 has high theoretical capacitance, but in practical applications its capacitance return is low and it can be attributed to poor electrical conductivity. The Co_3O_4 was coated with PANI and further the composite was coated with graphene. The coating of PANI over Co_3O_4 would increase charge collection through conducting channel networks and PANI would also contribute in pseudocapacitance through redox reactions. Co_3O_4 would also help to reduce the polymer backbone damage problem during charging-discharging process. To reduce the problem of shrinking and swelling and further increase electron transport pathways, Co_3O_4/polyaniline composite material was coated with graphene (graphene mainly contributes in electric double layer capacitance) [14, 32–36].

The electrochemical performances of the prepared Co_3O_4 nanoparticles and Co_3O_4/polyaniline/graphene composite were investigated. The composite material delivered high capacitance value with wide voltage window (− 0.8 to 0.8 V in three-electrode configuration) in presence of 1 M Na_2SO_4 aqueous electrolyte. Further, Co_3O_4/polyaniline/graphene was used to fabricate symmetric supercapacitors and their electrochemical performances were also investigated. It is also possible to increase the electrochemical performance by introducing redox additive (inorganic: KI, KBr, $VOSO_4$, $K_4Fe(CN)_6$, $CuSO_4$, $FeSO_4$, etc. and organic: hydroquinone, p-phenylenediamine, methylene blue, indigo carmine, etc.) into the electrolyte [37–44]. The redox additive improves the specific capacitance of supercapacitor via reversible redox reactions at the electrode/electrolyte interface and also intercalating and accumulating redox species inside the surface. Here, the effect of KI redox additive in 1 M Na_2SO_4 electrolyte in the fabricated symmetric supercapacitors, were also investigated.

2 Experimental

2.1 Preparation of Co_3O_4/polyaniline/graphene composite

All chemicals used in the experiments are listed in Supporting Information (SI). For the synthesis of Co_3O_4 nanoparticles, first 1 M 200 ml sodium hydroxide (NaOH) solution was added gradually under continuous stirring into 200 ml solution of 0.1 M cobalt (II) nitrate ($Co(NO_3)_2$). Then, the solution was kept stirring for 24 h at room temperature. The precipitate was separated by centrifugation and washed with deionized (DI) water and methanol repeatedly till the pH reached 7 and it was dried at 60 °C in a vacuum oven for 24 h. After that the product was calcined at 400 °C for 6 h with initial heating rate 5 °C/min.

As-prepared Co_3O_4 nanoparticles were used for the synthesis of composite material. To begin, 500 mg Co_3O_4 was added in 25 ml DI water and ultrasonicated for few minutes. After that 0.5 ml aniline was added in that solution and stirred for few minutes and next 25 ml 1 M H_2SO_4 was added slowly in the solution, followed by addition of 25 ml 0.2 M ammonium persulfate solution. The total solution was kept in room temperature and stirred for 24 h. The precipitate was separated by centrifugation and washed with DI water and methanol repeatedly and vacuum dried at 60 °C.

Next 300 mg GO (detail synthesis is discussed in SI) and 300 mg as prepared composite were added in 150 ml DI water and ultrasonicated for several minutes. Next 0.3 ml hydrazine hydrate was added in the mixture and kept stirring for 15 min. After that the mixture was refluxed in 100 °C for 24 h in silicone oil bath. Using methanol and DI water, the product was washed repeatedly to bring the pH neutral. Finally, the precipitate was dried for 24 h in a vacuum oven at 60 °C and the product was named as Co_3O_4/PANI/Graphene.

2.2 Material characterization

The X-ray diffraction patterns were obtained using a PANanalytical High-Resolution X-ray diffractometer (XRD), with Cu $K_{\alpha 1}$ radiation ($\lambda = 1.5406$ Å). The Raman measurements were conducted using Jobin Yvon Horiba T64000 Raman spectrometer (France) with an excitation wavelength of 514.5 nm. The Carl Zeiss SUPRA 40 field-emission scanning electron microscope (FESEM) and field-emission gun-transmission electron microscope (FEG-TEM) (model: JEM-2100F, JEOL) were used to investigate the particle morphology. The energy dispersive X-ray spectroscopy (EDS) elemental mapping data were collected using the Carl Zeiss AURIGA OXFORD-XMAX^N 50. A Quantachrome ChemBET (TPR/TPD) analyzer was used to measure the Brunauer–Emmett–Teller (BET) surface area of the materials.

2.3 Electrode preparation and electrochemical measurements

To prepare working electrodes, active material, acetylene black and PVDF-HFP were mixed in a mass ratio of 85:10:5, respectively, and the mixture was dispersed in acetone and stirred at 60 °C to get homogeneous slurry. The slurry was then drop-casted on current collector (graphite sheet (1×1 cm^2)) and dried for 12 h at 60 °C. The total mass loading maintained for Co_3O_4 and Co_3O_4/PANI/Graphene composite were 0.3–0.8 mg for electrochemical measurements in three-electrode cell system. Saturated Ag/AgCl (sat. KCl) and platinum (Pt) were used as reference and counter electrode, respectively. For the fabrication of two-electrode cell,

coin-cell CR 2032 and Whatman glass microfiber filter (separator) were used. The slurry drop-casted on graphite sheet (1×1 cm^2), used as positive and negative electrode (total mass loading of the both electrode was 0.8 mg i.e. effective mass 0.68 mg). The Metrohm Autolab (Galvanostat/Potentiostat) was used to study all electrochemical measurements.

3 Results and discussion

The XRD patterns of Co_3O_4 nanoparticles and Co_3O_4/PANI/Graphene composite are shown in Fig. 1. The phase formation of Co_3O_4 nanoparticles was confirmed by XRD and the peaks were indexed with JCPDS no. 42–1467 [45, 46]. The (511) peak of Co_3O_4 was clearly visible in Co_3O_4/PANI/Graphene composite. High amorphous matrix of PANI and graphene suppressed most of the sharp peaks of Co_3O_4 in Co_3O_4/PANI/Graphene composite. The Raman spectra of Co_3O_4 and Co_3O_4/PANI/Graphene are shown in Fig. S1. Prominent Raman peaks of Co_3O_4 were observed at 475, 516 and 680 cm^{-1} [47]. PANI and graphene in the composite Co_3O_4/PANI/Graphene, contributed in strong D and G band [48]. Figure 2 shows the FESEM and FEG-TEM images of Co_3O_4 and Co_3O_4/PANI/Graphene composite. The formation of Co_3O_4 nanoparticles was confirmed from the FESEM and FEG-TEM images (Fig. 2a and c, respectively). The coating of PANI and graphene were discernible in Co_3O_4/PANI/Graphene composite (shown in Fig. 2b, d). The elemental mapping of the composite material is shown in Fig. 3. Elemental mapping confirmed the uniform distributions of the constituent elements (in this case C, O, N and Co) in the composite material Co_3O_4/PANI/Graphene. Brunauer–Emmett–Teller (BET) N_2 adsorption–desorption isotherms and pore size distributions of Co_3O_4 nanomaterials and Co_3O_4/PANI/Graphene composite are shown in Fig. S2. Table 1 shows the comparison of pore diameter, pore volume and BET surface area of the samples. Due to the coating of PANI and graphene, the surface area and pore volume of Co_3O_4/PANI/Graphene composite were increased many folds compared to Co_3O_4 nanoparticles and the values were 132 m^2 g^{-1} and 0.19 cm^3 g^{-1}, respectively. The pores of the product were mesopores.

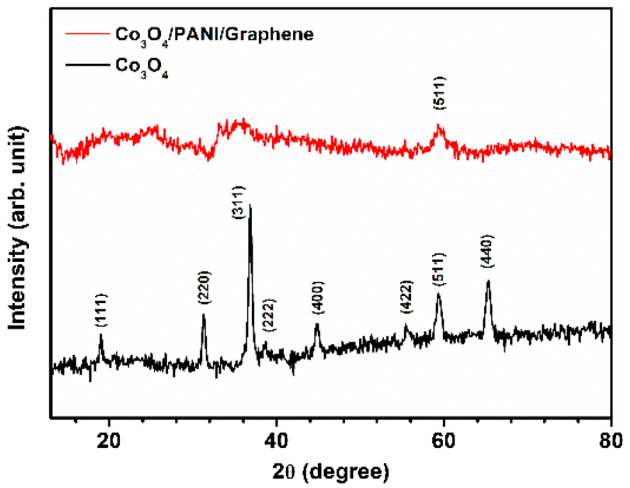

Fig. 1 XRD patterns of Co_3O_4 nanoparticles and Co_3O_4/PANI/Graphene composite

The equations used for calculating capacitance of the supercapacitors are shown in SI. Electrochemical measurements of Co_3O_4 in three-electrode configuration are discussed in SI. Extended operating voltage (− 0.8 to 0.8 V) was observed using 1 M Na_2SO_4 electrolyte. The strongly solvated sulfate anions and cations and well-maintained $H^+|OH^-$ equilibrium (due to neutral electrolyte) in 1 M Na_2SO_4 electrolyte, cumulatively effect in high decomposition voltage of the electrolyte [5]. Specific capacitance obtained from cyclic voltammetry (CV) curve was ~ 110 F g^{-1} (at a scan rate 5 mV s^{-1}). From galvanostatic charge–discharge (CD) curve, the value was ~ 150 F g^{-1} (at a current density 1 A g^{-1}).

The three-electrode electrochemical measurements of Co_3O_4/PANI/Graphene composite in 1 M Na_2SO_4 electrolyte (within the voltage window from − 0.8 to 0.8 V) are shown in Fig. 4. Figure 4a, b shows the CV measurements (at different scan rates) and CD measurements (at different current densities). For Co_3O_4/PANI/Graphene composite, the maximum specific capacitance achieved from CV and CD were ~ 313 F g^{-1} (at a scan rate 5 mV s^{-1}) and ~ 476 F g^{-1} (at a current density 2 A g^{-1}), respectively. The capacitance values procured from CV and CD for Co_3O_4/PANI/Graphene were increased more than 3 times, compared to Co_3O_4 nanoparticles and this was due to the effect of PANI and graphene coating on Co_3O_4 nanoparticles. Being a conducting polymer PANI contribute in pseudocapacitance and graphene provide EDLC and conducting pathways to transport electrons. Further, Co_3O_4 nanoparticles contributes not only as pseudocapacitance material but also solve the polymer backbone damage problem. The surface area of Co_3O_4/PANI/Graphene (132 m^2 g^{-1}) was very high compared to Co_3O_4 nanoparticles (34 m^2 g^{-1}) which resulted in increased capacitance by allowing extra space for redox reactions, ion intercalation/deintercalation and formation of electric double layer. The redox reactions of Co_3O_4/PANI/Graphene can be explained by the following equations [36]:

$$Co_3O_4 + \delta M^+ + \delta e^- \leftrightarrow M_\delta Co_3O_4 (\rightarrow \text{during discharging}) \quad (1)$$

$$PANI + \delta M^+ + \delta e^- \leftrightarrow (M^+)_\delta\ PANI^{\delta-} \quad (2)$$

$$PANI + \delta A^- \leftrightarrow PANI^{\delta+}(A^-)_\delta + \delta e^- \quad (3)$$

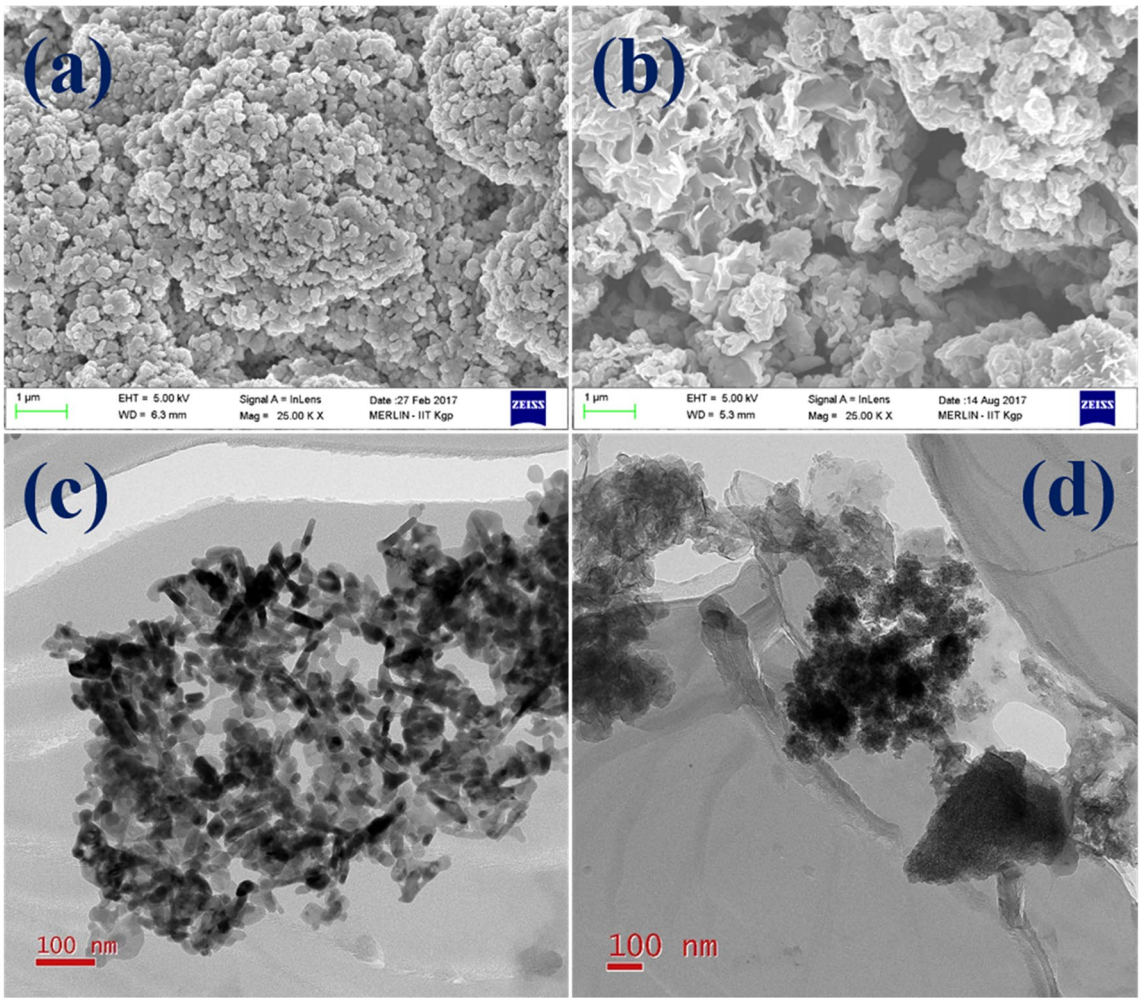

Fig. 2 FESEM images of **a** Co_3O_4 nanoparticles and **b** Co_3O_4/PANI/Graphene composite and FEG-TEM images of **c** Co_3O_4 nanoparticles and **d** Co_3O_4/PANI/Graphene composite

where M^+ represents the alkali metal cations (here it is Na^+) and protons and A^- denotes the anions in the electrolyte.

Figure 4c, d depicts the scan rate vs specific capacitance and specific current vs specific capacitance plots, respectively. The decreasing trend of capacitance was observed with increasing scan rates and specific currents. Cycling was done at a current density 17.5 A g^{-1} (shown in Fig. S4) and after 3000 cycles capacitance retention was found to be ~ 112%.

Further, the electrochemical measurements Co_3O_4/PANI/Graphene composite were investigated in symmetric two-electrode coin-cell devices (the details are discussed in SI). The voltage window was from 0 to 1.6 V. Specific capacitance obtained from CV and CD were ~ 34 F g^{-1} (at a scan rate 5 mV s^{-1}) and ~ 37 F g^{-1} (at a current density 0.5 A g^{-1}), respectively.

The effect of redox additive (KI) in 1 M Na_2SO_4 electrolyte in symmetric two-electrode coin-cell devices, prepared using Co_3O_4/PANI/Graphene composite was further investigated. Different concentrations of KI were used in 1 M Na_2SO_4 electrolyte and total mass of the electrode (including positive and negative electrode) was kept 0.8–1 mg during fabrication of symmetric coin cells. Figure 5 shows the CV curves at various scan rates of symmetric cells prepared using different concentrations of KI (20, 50, 75 and 100 mmol) in 1 M Na_2SO_4. The shape of the CV curves changed with addition of KI, compared to the situation when KI was not added in electrolyte (shown in Fig. S5(b)) and also redox peak was observed, when KI was added. Figure 6 shows the CD curves at different specific currents for different concentrations of KI (20, 50, 75 and 100 mmol), added in 1 M Na_2SO_4. Figure S7 shows the comparison of CV curves at different concentration of KI, at scan rate 5, 20,

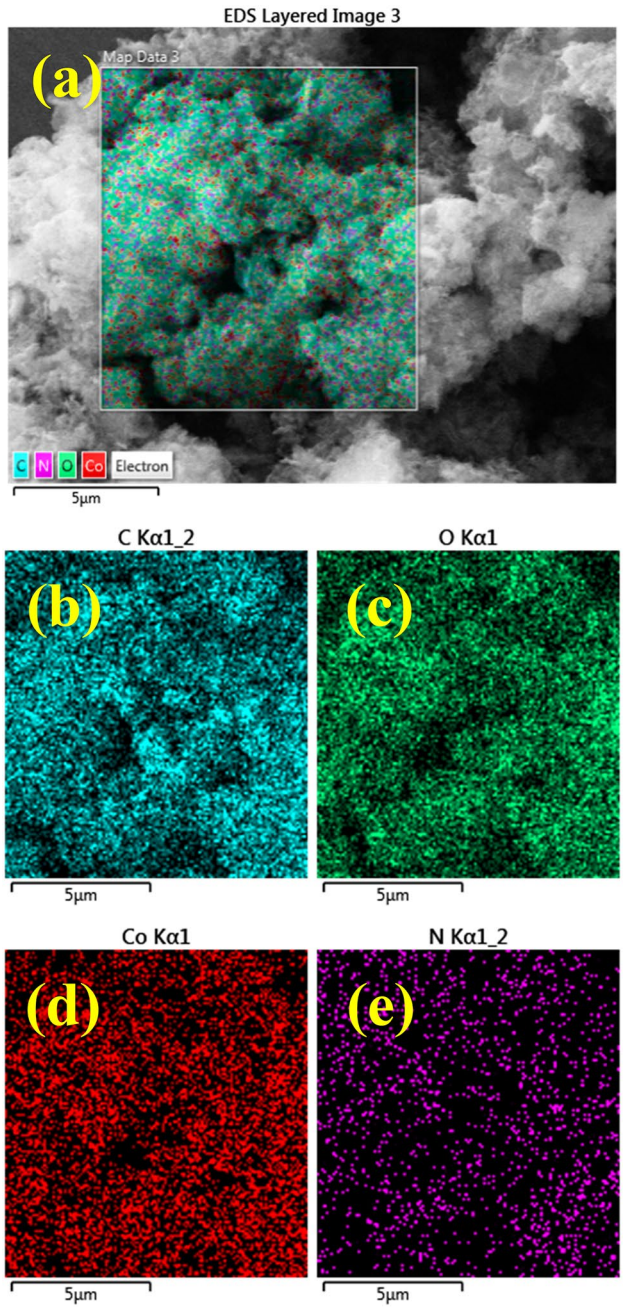

Fig. 3 Elemental mapping of Co_3O_4/PANI/Graphene: **a** overall, **b** C, **c** O, **d** Co and **e** N distributions

Table 1 Comparison of pore diameter, pore volume and BET surface area of the samples

Sample	Pore diameter (nm)	Pore volume (cm^3 g^{-1})	Surface area (m^2 g^{-1})
Co_3O_4	3	0.05	34
Co_3O_4/PANI/Graphene	3	0.19	132

50 and 100 mV s^{-1}. With increasing the KI concentration in 1 M Na_2SO_4 electrolyte, the area under CV curve increased upto addition of 75 mmol KI and after that in 100 mmol KI, it did not increase significantly. Furthermore, this trend was confirmed by CD curves of symmetric cells at different concentration of KI at specific current 2, 3, 4 and 5 A g^{-1} (shown in Fig. S8). Figure 7a shows the scan rate vs specific capacitance and 7b shows the specific current vs specific capacitance plot of symmetric cell at different concentration of KI. From Fig. 7, it was inferred that in the case of 75 mmol KI in 1 M Na_2SO_4, the capacitance was maximum and after that with increased KI concentration, the capacitance decreased. The maximum capacitance calculated for symmetric cell using 75 mmol KI in 1 M Na_2SO_4, was ~ 70 F g^{-1}, at a scan rate 5 mV s^{-1} from CV and from CD, capacitance was ~ 94 F g^{-1}, at a current density 1 A g^{-1}. With addition of redox additive 75 mmol KI in 1 M Na_2SO_4, the capacitance increased more than double, calculated from CV and CD, compared to when only 1 M Na_2SO_4 electrolyte was used. The increase of capacitance with addition of KI in 1 M Na_2SO_4 electrolyte, can be attributed to the redox reactions of the adsorbed redox species (in this case polyiodide) on the internal and external surfaces of the electrode and also intercalating and accumulating redox species inside the surface. As the Co_3O_4/PANI/Graphene composite was mesoporous (average pore diameter 3 nm), the solvated iodine species (i.e. polyiodides) of size ~ 1.8 nm can easily accumulate and intercalate inside the surface and high surface area of Co_3O_4/PANI/Graphene composite (132 m^2 g^{-1}) provide platform for redox reactions to take place on the surface of electrode. The redox reactions are given below [39]:

$$3I^- \leftrightarrow I_3^- + 2e^- \quad (4)$$

$$2I^- \leftrightarrow I_2 + 2e^- \quad (5)$$

$$2I_3^- \leftrightarrow 3I_2 + 2e^- \quad (6)$$

$$I_2 + 6H_2O \leftrightarrow 2IO_3^- + 12H^+ + 10e^- \quad (7)$$

On increasing the concentration of KI from 75 to 100 mmol, the excess concentration of KI would not contribute in high capacitance. This can be attributed to the fact that excess KI concentration would cause strong repulsion between iodine and polyiodide ions which causes the decrease in adsorption and faradaic reactions [39, 44]. The comparison of Nyquist plot of symmetric cells in different concentrations of KI are depicted in Fig. S9. From the inset of Fig. S9, it was clear that the optimum system showed lowest ion charge transfer resistance, which also contributes in getting high capacitance value. Figure 8 shows the comparison of cycles vs specific

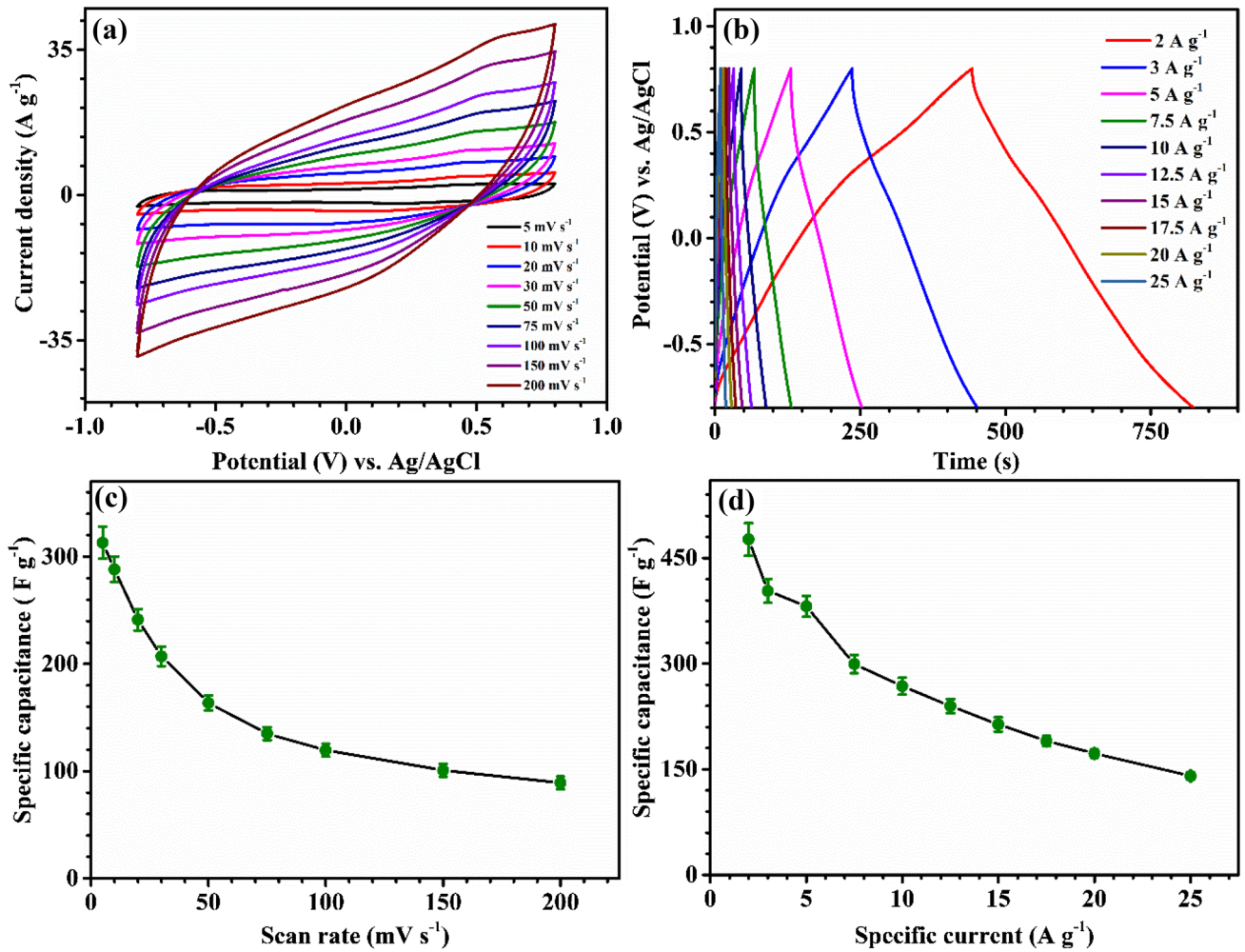

Fig. 4 Electrochemical measurements of Co_3O_4/PANI/Graphene in three-electrode configuration: **a** CV curves at various scan rates, **b** CD curves at different specific currents, **c** scan rate vs specific capacitance plot and **d** specific current vs specific capacitance plot

capacitance plot of symmetric cell for different concentration of KI and for optimum system the capacitance retention was found to be ~ 78%. The comparison of Ragone plots are depicted in Fig. 9. For optimum system, the energy density and power density calculated were found to be 33.5 W h kg^{-1} and 800 W kg^{-1}, respectively, at a current density 1 A g^{-1} which was more than two times higher than the case when no redox additive was added. The energy density and power density calculated for Co_3O_4/PANI/Graphene//Co_3O_4/PANI/Graphene symmetric supercapacitor (electrolyte: 75 mmol KI in 1 M Na_2SO_4) were greater than previously reported symmetric supercapacitors. The comparison is given in the Table 2.

4 Conclusions

Co_3O_4/PANI/Graphene composite showed high capacitance value and stable wide voltage window (ranging from − 0.8 to 0.8 V), using 1 M Na_2SO_4 as neutral aqueous electrolyte during three-electrode measurement. The

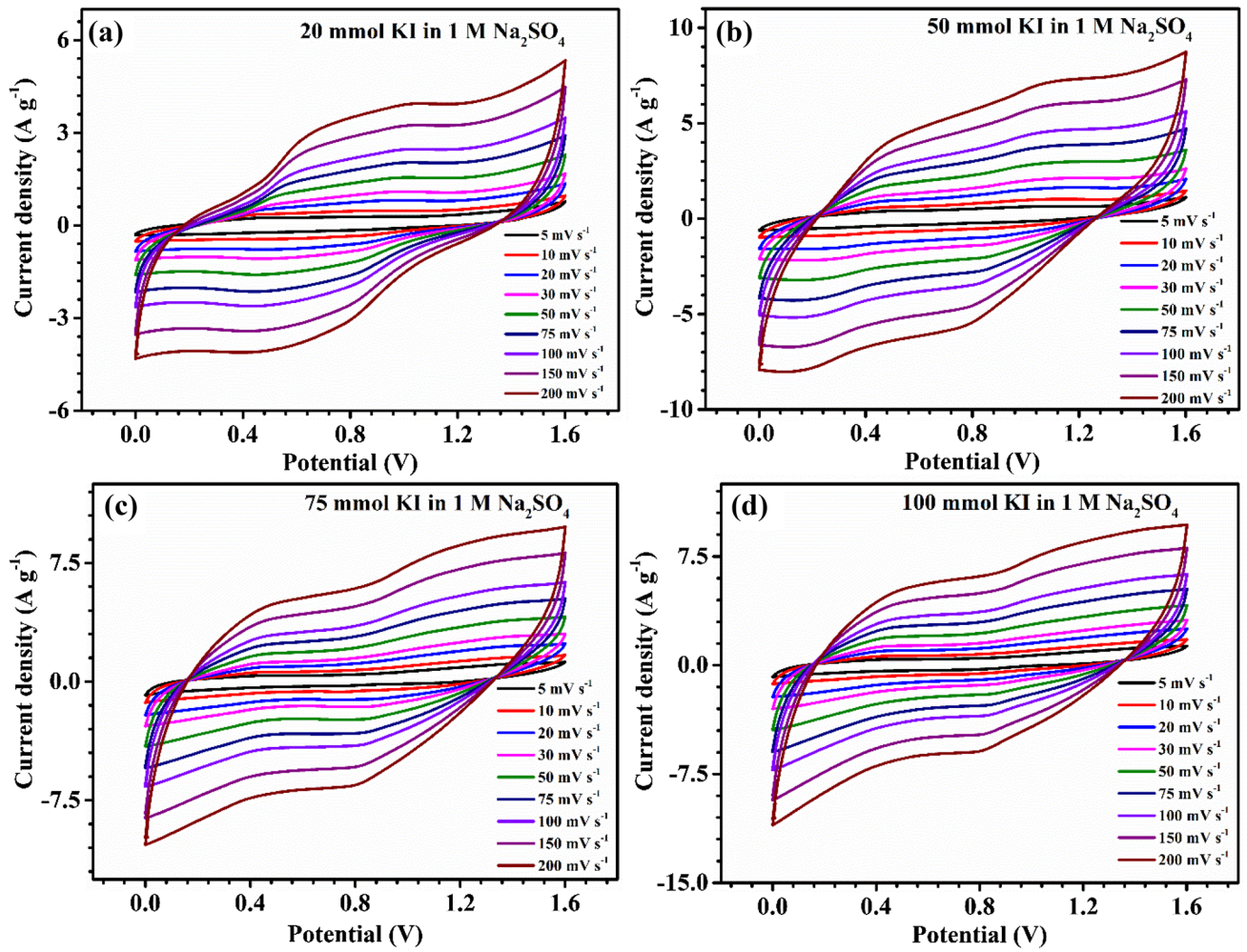

Fig. 5 CV curves at various scan rates of symmetric cells prepared using Co_3O_4/PANI/Graphene after addition of **a** 20 mmol, **b** 50 mmol, **c** 75 mmol and **d** 100 mmol KI in 1 M Na_2SO_4 electrolyte, respectively

highest capacitance obtained from CD was ~ 476 F g^{-1} (at a current density 2 A g^{-1}) and showed ~ 112% capacitance retention after 3000 cycles (@ 17.5 A g^{-1}). Furthermore, Co_3O_4/PANI/Graphene composite was used to configure symmetric cell and the cell operated within the voltage window 0–1.6 V. The highest capacitance obtained from CD curve for symmetric cell was ~ 37 F g^{-1} (at a current density 0.5 A g^{-1}) and the cycling stability was found to be very good (~ 94%). The effect of redox additive KI in electrolyte 1 M Na_2SO_4 of the symmetric device was investigated. Optimum results were obtained for 75 mmol KI added in 1 M Na_2SO_4 electrolyte and the increment of capacitance was more than two times, compared to the case where no redox additive was added in electrolyte and the maximum capacitance was found to be ~ 94 F g^{-1} from CD (at a current density 1 A g^{-1}). The energy density and

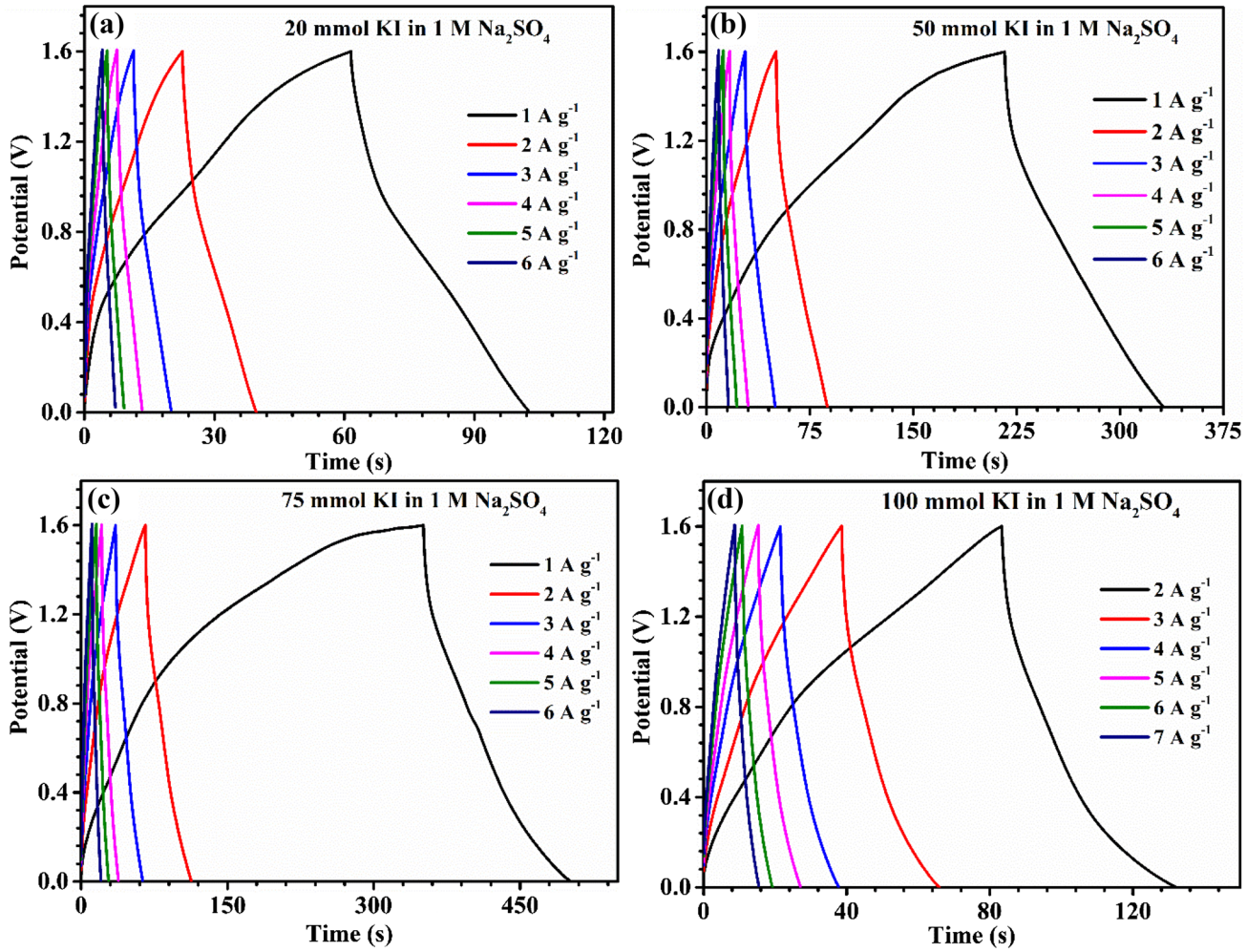

Fig. 6 CD curves at different specific currents of symmetric cells prepared using Co_3O_4/PANI/Graphene after addition of **a** 20 mmol, **b** 50 mmol, **c** 75 mmol and **d** 100 mmol KI in 1 M Na_2SO_4 electrolyte, respectively

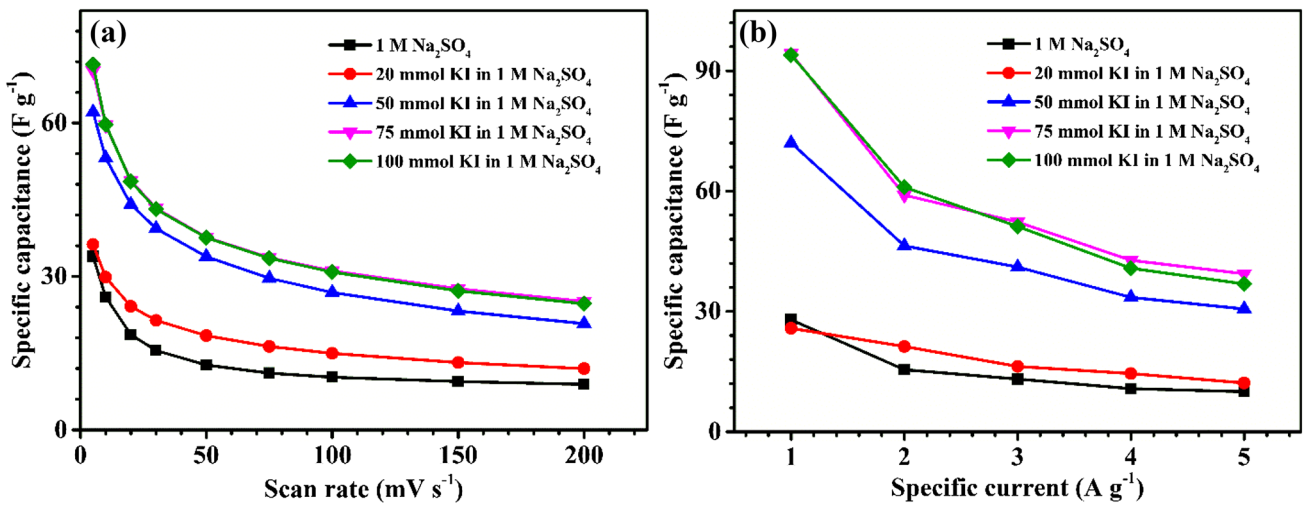

Fig. 7 Comparison of **a** scan rate vs specific capacitance and **b** specific current vs specific capacitance plots of symmetric cells prepared using Co_3O_4/PANI/Graphene in different concentrations of KI

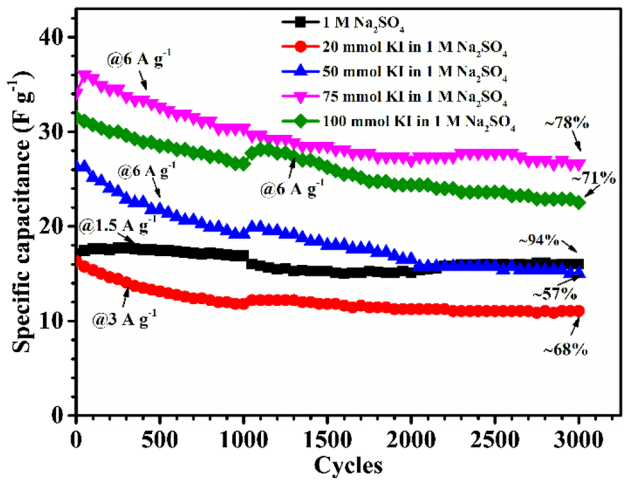

Fig. 8 Comparison of cycles vs specific capacitance plot of symmetric cells prepared using Co_3O_4/PANI/Graphene in different concentrations of KI

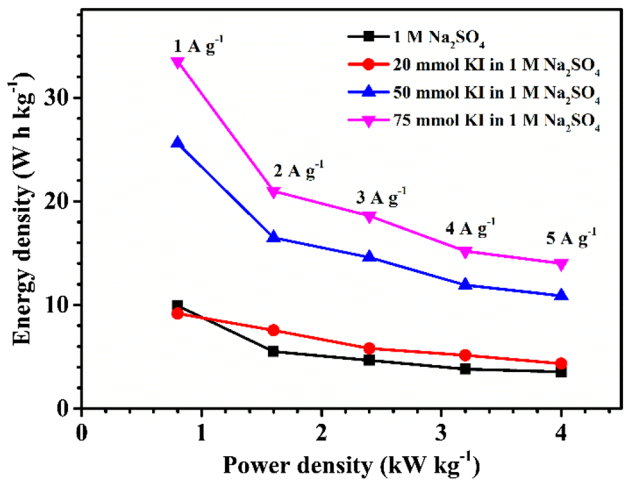

Fig. 9 Comparison of Ragone plot of symmetric cells prepared using Co_3O_4/PANI/Graphene in different concentrations of KI

power density achieved (at a current density 1 A g^{-1}) were 33.5 W h kg^{-1} and 800 W kg^{-1}, respectively.

Acknowledgements Prasenjit Haldar (PH) acknowledges University Grants Commission (UGC), India for providing Senior Research Fellowship. Special thanks to Dr. Amreesh Chandra (Professor of Department of Physics, Indian Institute of Technology Kharagpur, India), for introducing PH to the field of supercapacitors.

References

1. C. Masarapu, H.F. Zeng, K.H. Hung, B. Wei, Effect of temperature on the capacitance of carbon nanotube supercapacitors. ACS Nano **3**, 2199–2206 (2009)
2. R. German, O. Briat, A. Sari, P. Venet, M. Ayadi, Y. Zitouni, J.M. Vinassa, Impact of high frequency current ripple on supercapacitors ageing through floating ageing tests. Microelectron. Reliab. **53**, 1643–1647 (2013)
3. Z. Zeng, Y. Liu, W. Zhang, H. Chevva, J. Wei, Improved supercapacitor performance of MnO_2-electrospun carbon nanofibers electrodes by mT magnetic field. J. Power Sources **358**, 22–28 (2017)
4. P. Haldar, S. Biswas, V. Sharma, A. Chandra, Understanding the origin of magnetic field dependent specific capacitance in Mn_3O_4 nanoparticle based supercapacitors. J. Electrochem. Soc. **165**, A3230–A3239 (2018)
5. K. Fic, G. Lota, M. Meller, E. Frackowiak, Novel insight into neutral medium as electrolyte for high-voltage supercapacitors. Energy Environ. Sci. **5**, 5842–5850 (2012)
6. Q. Wang, J. Yan, Y. Wang, G. Ning, Z. Fan, T. Wei, J. Cheng, M. Zhang, X. Jing, Template synthesis of hollow carbon spheres anchored on carbon nanotubes for high rate performance supercapacitors. Carbon **52**, 209–218 (2013)
7. V. Sharma, S. Biswas, B. Sundaram, P. Haldar, B. Dubey, A. Chandra, Electrode materials with highest surface area and specific capacitance cannot be the only deciding factor for applicability in energy storage devices: inference of combined life cycle assessment and electrochemical studies. ACS Sustain. Chem. Eng. **7**, 5385–5392 (2019)
8. A.K. Thakur, R.B. Choudhary, High-performance supercapacitors based on polymeric binary composites of polythiophene (PTP)–titanium dioxide (TiO_2). Synth. Met. **220**, 25–33 (2016)
9. Y. Gao, Graphene and polymer composites for supercapacitor applications: a review. Nanoscale Res. Lett. **12**, 387 (2017)

Table 2 Comparison of energy density and power density between previously reported work and present work in symmetric cell configuration

Symmetric device	Energy density (W h kg^{-1})	Power density(W kg^{-1})	Reference
VN/PCNPs//VN/PCNPs	8.0	575	[49]
FeS//FeS	2.6	726	[50]
HPDC-7//HPDC-7	21.5	440	[51]
Glu-2.5//Glu-2.5	16.7	404.7	[52]
VO_2//VO_2	21.3	207.2	[53]
NPC//NPC	10.9	225	[54]
Cu_2O/Cu//Cu_2O/Cu	24.0	625	[55]
$MnFe_2O_4$/rGO//$MnFe_2O_4$/rGO	15.9	324.5	[56]
Fe_3O_4-GNS//Fe_3O_4-GNS	11.0	200	[57]
Co_3O_4/PANI/Graphene//Co_3O_4/PANI/Graphene (electrolyte: 75 mmol KI in 1 M Na_2SO_4)	33.5	800	Present work

10. X. Wang, D. Wu, X. Song, W. Du, X. Zhao, D. Zhang, Review on carbon/polyaniline hybrids: design and synthesis for supercapacitor. Molecules **24**, 2263 (2019)
11. L. Fu, Q. Qu, R. Holze, V.V. Kondratiev, Y. Wu, Composites of metal oxides and intrinsically conducting polymers as supercapacitor electrode materials: the best of both worlds? J. Mater. Chem. A. **7**, 14937–14970 (2019)
12. Y.-R. Zhu, P.-P. Peng, J.-Z. Wu, T.-F. Yi, Y. Xie, S. Luo, Co_3O_4@ $NiCo_2O_4$ microsphere as electrode materials for high-performance supercapacitors. Solid State Ionics **336**, 110–119 (2019)
13. A.K. Thakur, A.B. Deshmukh, R.B. Choudhary, I. Karbhal, M. Majumder, M.V. Shelke, Facile synthesis and electrochemical evaluation of PANI/CNT/MoS_2 ternary composite as an electrode material for high performance supercapacitor. Mater. Sci. Eng. B. **223**, 24–34 (2017)
14. G. Han, Y. Liu, L. Zhang, E. Kan, S. Zhang, J. Tang, W. Tang, MnO_2 Nanorods intercalating graphene oxide/polyaniline ternary composites for robust high-performance supercapacitors. Sci. Rep. **4**, 4824 (2014)
15. M. Kazazi, High-performance electrode based on electrochemical polymerization of polypyrrole film on electrophoretically deposited CNTs conductive framework for supercapacitors. Solid State Ionics **336**, 80–86 (2019)
16. X. Jiang, Y. Cao, P. Li, J. Wei, K. Wang, D. Wu, H. Zhu, Polyaniline/graphene/carbon fiber ternary composites as supercapacitor electrodes. Mater. Lett. **140**, 43–47 (2015)
17. E.-C. Cho, C.-W. Chang-Jian, K.-C. Lee, J.-H. Huang, B.-C. Ho, R.-Z. Liu, Y.-S. Hsiao, Ternary composite based on homogeneous $Ni(OH)_2$ on graphene with Ag nanoparticles as nanospacers for efficient supercapacitor. Chem. Eng. J. **334**, 2058–2067 (2018)
18. L. Yue, S. Zhang, H. Zhao, Y. Feng, M. Wang, L. An, X. Zhang, J. Mi, One-pot synthesis $CoFe_2O_4$/CNTs composite for asymmetric supercapacitor electrode. Solid State Ionics **329**, 15–24 (2019)
19. L. Wang, T. Wu, S. Du, M. Pei, W. Guo, S. Wei, High performance supercapacitors based on ternary graphene/Au/polyaniline (PANI) hierarchical nanocomposites. RSC Adv. **6**, 1004–1011 (2016)
20. N.H.N. Azman, M.S. Mamat @ Mat Nazir, L.H. Ngee, Y. Sulaiman, Graphene-based ternary composites for supercapacitors. Int. J. Energy Res. **42**, 2104–2116 (2018)
21. J. Qi, D. Chen, W. Wang, Y. Sui, Y. He, Q. Meng, F. Wei, Y. Ren, J. Liu, Y. Jin, Facile synthesis of N-doped activated carbon derived from cotton and $CuCo_2O_4$ nanoneedle arrays electrodes for all-solid-state asymmetric supercapacitor. J. Mater. Sci. Mater. Electron. **30**, 9877–9887 (2019)
22. Z. Wang, H.Y. Yue, Z.M. Yu, F. Yao, X. Gao, E.H. Guan, H.J. Zhang, W.Q. Wang, S.S. Song, One-pot hydrothermal synthesis of $MoSe_2$ nanosheets spheres-reduced graphene oxide composites and application for high-performance supercapacitor. J. Mater. Sci. Mater. Electron. **30**, 8537–8545 (2019)
23. L. Tao, L. Shengjun, Z. Bowen, W. Bei, N. Dayong, C. Zeng, Y. Ying, W. Ning, Z. Weifeng, Supercapacitor electrode with a homogeneously Co_3O_4-coated multiwalled carbon nanotube for a high capacitance. Nanoscale Res. Lett. **10**, 208 (2015)
24. C. Yuan, L. Yang, L. Hou, L. Shen, X. Zhang, X.W. Lou, Growth of ultrathin mesoporous Co_3O_4 nanosheet arrays on Ni foam for high-performance electrochemical capacitors. Energy Environ. Sci. **5**, 7883–7887 (2012)
25. H. Cheng, Z.G. Lu, J.Q. Deng, C.Y. Chung, K. Zhang, Y.Y. Li, A facile method to improve the high rate capability of Co_3O_4 nanowire array electrodes. Nano Res. **3**, 895–901 (2010)
26. X. Sun, Z. Jiang, C. Li, Y. Jiang, X. Sun, X. Tian, L. Luo, X. Hao, Z.-J. Jiang, Facile synthesis of Co_3O_4 with different morphologies loaded on amine modified graphene and their application in supercapacitors. J. Alloys Compd. **685**, 507–517 (2016)
27. H. Chen, M. Yang, S. Tao, M. Ren, G. Chen, Facile synthesis of Co_3O_4 with different morphologies via oxidation kinetic control and its application in hydrogen peroxide decomposition. Cryst. Growth Des. **16**, 6286–6293 (2016)
28. C. Yuan, L. Yang, L. Hou, L. Shen, F. Zhang, D. Li, X. Zhang, Large-scale Co_3O_4 nanoparticles growing on nickel sheets via a one-step strategy and their ultra-highly reversible redox reaction toward supercapacitors. J. Mater. Chem. **21**, 18183–18185 (2011)
29. Y.Q. Zhang, L. Li, S.J. Shi, Q.Q. Xiong, X.Y. Zhao, X.L. Wang, C.D. Gu, J.P. Tu, Synthesis of porous Co_3O_4 nanoflake array and its temperature behavior as pseudo-capacitor electrode. J. Power Sources **256**, 200–205 (2014)
30. B. Vidyadharan, R.A. Aziz, I.I. Misnon, G.M. Anil Kumar, J. Ismail, M.M. Yusoff, R. Jose, High energy and power density asymmetric supercapacitors using electrospun cobalt oxide nanowire anode. J. Power Sources **270**, 526–535 (2014)
31. J. Sun, Y. Wang, Y. Zhang, C. Xu, H. Chen, Egg albumin-assisted hydrothermal synthesis of Co_3O_4 quasi-cubes as superior electrode material for supercapacitors with excellent performances. Nanoscale Res. Lett. **14**, 340 (2019)
32. H. Wang, J. Lin, Z.X. Shen, Polyaniline (PANi) based electrode materials for energy storage and conversion. J. Sci. Adv. Mater. Devices **1**, 225–255 (2016)
33. Y. Wang, S. Tang, S. Vongehr, J. AliSyed, X. Wang, X. Meng, High-Performance flexible solid-state carbon cloth supercapacitors based on highly processible N-graphene doped polyacrylic acid/polyaniline composites. Sci. Rep. **6**, 12883 (2016)
34. Y. Shi, L. Peng, Y. Ding, Y. Zhao, G. Yu, Nanostructured conductive polymers for advanced energy storage. Chem. Soc. Rev. **44**, 6684–6696 (2015)
35. M. Notarianni, J. Liu, F. Mirri, M. Pasquali, N. Motta, Graphene-based supercapacitor with carbon nanotube film as highly efficient current collector. Nanotechnology. **25**, 435405 (2014)
36. P. Haldar, S. Biswas, V. Sharma, A. Chowdhury, A. Chandra, Mn_3O_4-polyaniline-graphene as distinctive composite for use in high-performance supercapacitors. Appl. Surf. Sci. **491**, 171–179 (2019)
37. C. Zhong, Y. Deng, W. Hu, J. Qiao, L. Zhang, J. Zhang, A review of electrolyte materials and compositions for electrochemical supercapacitors. Chem. Soc. Rev. **44**, 7484–7539 (2015)
38. N.R. Chodankar, D.P. Dubal, A.C. Lokhande, A.M. Patil, J.H. Kim, C.D. Lokhande, An innovative concept of use of redox-active electrolyte in asymmetric capacitor based on MWCNTs/MnO_2 and Fe_2O_3 thin films. Sci. Rep. **6**, 39205 (2016)
39. A. Singh, A. Chandra, Enhancing specific energy and power in asymmetric supercapacitors—a synergetic strategy based on the use of redox additive electrolytes. Sci. Rep. **6**, 25793 (2016)
40. D. Jain, J. Kanungo, S.K. Tripathi, Enhanced performance of ultracapacitors using redox additive-based electrolytes. Appl. Phys. A. **124**, 397 (2018)
41. D. Xu, W. Hu, X.N. Sun, P. Cui, X.Y. Chen, Redox additives of Na_2MoO_4 and KI: synergistic effect and the improved capacitive performances for carbon-based supercapacitors. J. Power Sources. **341**, 448–456 (2017)
42. Z. Khan, B. Senthilkumar, S. Lim, R. Shanker, Y. Kim, H. Ko, Redox-Additive-enhanced high capacitance supercapacitors based on $Co_2P_2O_7$ nanosheets. Adv. Mater. Interfaces **4**, 1700059 (2017)
43. B. Akinwolemiwa, C. Peng, G.Z. Chen, Redox electrolytes in supercapacitors. J. Electrochem. Soc. **162**, A5054–A5059 (2015)
44. S.T. Senthilkumar, R.K. Selvan, J.S. Melo, Redox additive/active electrolytes: a novel approach to enhance the performance of supercapacitors. J. Mater. Chem. A **1**, 12386–12394 (2013)
45. X. Liu, Q. Long, C. Jiang, B. Zhan, C. Li, S. Liu, Q. Zhao, W. Huang, X. Dong, Facile and green synthesis of mesoporous Co_3O_4

nanocubes and their applications for supercapacitors. Nanoscale. **5**, 6525–6529 (2013)
46. X. Wang, L. Yu, X.-L. Wu, F. Yuan, Y.-G. Guo, Y. Ma, J. Yao, Synthesis of single-crystalline Co_3O_4 octahedral cages with tunable surface aperture and their lithium storage properties. J. Phys. Chem. C **113**, 15553–15558 (2009)
47. R.B. Rakhi, W. Chen, D. Cha, H.N. Alshareef, Substrate dependent self-organization of mesoporous cobalt oxide nanowires with remarkable pseudocapacitance. Nano Lett. **12**, 2559–2567 (2012)
48. B. Rajagopalan, S.H. Hur, J.S. Chung, Surfactant-treated graphene covered polyaniline nanowires for supercapacitor electrode. Nanoscale Res. Lett. **10**, 183 (2015)
49. Y. Yang, K. Shen, Y. Liu, Y. Tan, X. Zhao, J. Wu, X. Niu, F. Ran, Novel hybrid nanoparticles of vanadium nitride/porous carbon as an anode material for symmetrical supercapacitor. Nano-Micro Lett. **9**(1), 6 (2016)
50. S.S. Karade, P. Dwivedi, S. Majumder, B. Pandit, B.R. Sankapal, First report on a FeS-based 2 V operating flexible solid-state symmetric supercapacitor device. Sustain. Energy Fuels **1**, 1366–1375 (2017)
51. H. Li, G. Zhang, R. Zhang, H. Luo, L. Wang, C. Hu, I. Samo, Y. Pang, Z. Chang, X. Sun, Scalable fabrication of hierarchically porous N-doped carbon electrode materials for high-performance aqueous symmetric supercapacitor. J. Mater. Sci. **53**, 5194–5203 (2017)
52. G. Ma, Z. Zhang, H. Peng, K. Sun, F. Ran, Z. Lei, Facile preparation of nitrogen-doped porous carbon for high performance symmetric supercapacitor. J. Solid State Electrochem. **20**, 1613–1623 (2016)
53. X.-J. Ma, W.-B. Zhang, L.-B. Kong, Y.-C. Luo, L. Kang, VO_2: from negative electrode material to symmetric electrochemical capacitor. RSC Adv. **5**, 97239–97247 (2015)
54. R.R. Salunkhe, Y. Kamachi, N.L. Torad, S.M. Hwang, Z. Sun, S.X. Dou, J.H. Kim, Y. Yamauchi, Fabrication of symmetric supercapacitors based on MOF-derived nanoporous carbons. J. Mater. Chem. A. **2**, 19848–19854 (2014)
55. C. Wan, Y. Jiao, J. Li, A cellulose fibers-supported hierarchical forest-like cuprous oxide/copper array architecture as a flexible and free-standing electrode for symmetric supercapacitors. J. Mater. Chem. A. **5**, 17267–17278 (2017)
56. A. GoljanianTabrizi, N. Arsalani, A. Mohammadi, H. Namazi, L. SalehGhadimi, I. Ahadzadeh, Facile synthesis of a $MnFe_2O_4$/rGO nanocomposite for an ultra-stable symmetric supercapacitor. New J. Chem. **41**, 4974–4984 (2017)
57. K. Karthikeyan, D. Kalpana, S. Amaresh, Y.S. Lee, Microwave synthesis of graphene/magnetite composite electrode material for symmetric supercapacitor with superior rate performance. RSC Adv. **2**, 12322–12328 (2012)